Journal of Materials Science: Materials in Electronics
https://doi.org/10.1007/s10854-019-01974-x

Electrical properties and defect compensation mechanism of B-site Cu^{2+} substituted $K_{0.5}Na_{0.5}NbO_3$ ceramics

Pengrong Ren[1] · Yike Wang[1] · Jiale Wang[1] · Dong Ren[1] · Liang Sun[2] · Xiao Liu[3] · Fuxue Yan[1] · Gaoyang Zhao[1]

Received: 29 April 2019 / Accepted: 1 August 2019

Abstract
Cu^{2+} substituted $K_{0.5}Na_{0.5}NbO_3$ ceramics at B-site $K_{0.5}Na_{0.5}(Nb_{1-x}Cu_x)O_{3-3x/2}$ (KNNC) were prepared by a solid state method. The dielectric, ferroelectric properties and defect compensation mechanism were studied. With the concentration of Cu^{2+} increasing from 0.005 to 0.10, permittivity and dielectric loss decrease, but further increasing the concentration of Cu^{2+} increasing leads to the increment of permittivity and dielectric loss. All KNNC ceramics exhibit double hysteresis loop characteristics. When the doping concentration Cu^{2+} is low (x = 0.0075), the double hysteresis loop disappears at large electric field, nonetheless, when x = 0.015, it maintains the characteristics of the double hysteresis loop even under the high electric field. The corresponding mechanism is explained from the aspects of correlation between defect dipoles and polarization orientation.

1 Introduction

Piezoelectric ceramics have important applications in actuator, transducer and sensor [1]. Currently, $Pb(Zr_xTi_{1-x})O_3$ (PZT) with the MPB composition of x = 0.52 is the dominant piezoelectric ceramic in the commercial market. For high-power ultrasonic applications, it is usually doped by a variety of acceptor ions to form what are known as "hard" PZTs. Because acceptor doping results in defects dipoles, which create an internal electric field, pin the domain wall and reduce domain wall mobility, "hard" PZTs have higher mechanical quality factor (Q_m), lower dielectric loss and lower hysteresis in polarization–electric field (P–E) loop [2, 3]. However, PZT constitutes a large fraction of hazardous lead oxide. Driven by environmental regulations such as WEEE (waste of electrical and electronic equipment) and RoHS (restriction of certain hazardous substances), lead-free piezoelectric ceramics have been actively studied in recent years [4].

In general, $K_{0.5}Na_{0.5}NbO_3$ (KNN) belongs to the "soft" piezoelectric ceramic, with high loss, low Q_m and modest coercive field ($E_C \approx 5$–9 kV/cm) [5, 6]. However, some ions are doped to KNN to make it as a "hard" piezoelectric ceramic. Cu^{2+} (and/or Cu^{+}) is a special element. On the one hand, it was reported that addition of CuO could improve mechanical quality factor (Q_m) of KNN ceramics [7]. On the other hand, CuO could be served as a sintering aid to increase the density of KNN ceramics [8]. Although the addition of CuO in KNN has been reported by many researchers, doping position and defect compensation mechanism due to isovalent substitution of Cu^{2+} in KNN ceramics are still debated. Some researchers argued that the doping position is dependent on oxygen partial pressures and A-site vacancy concentrations. When oxygen partial pressure is low, Cu element preferentially substitutes K^+ or Na^+ in the form of Cu^+ priority, nevertheless, when oxygen partial pressure is high, Cu element substitutes Nb^{5+} in the form of Cu^{2+} [9, 10]. Furthermore, when K^+ or Na^+ is highly absent, Cu^{2+} preferentially substitutes K^+ or Na^+, otherwise Cu^{2+} preferentially substitutes Nb^{5+} [7, 9, 10]. In addition, double ferroelectric hysteresis loops are reported in Cu^{2+} doped KNN by different researchers [11, 12]. And this behavior is largely dependent on the doping

✉ Pengrong Ren
renpengrongxaut@126.com

[1] Shaanxi Province Key Laboratory for Electrical Materials and Infiltration Technology, School of Materials Science and Engineering, Xi'an University of Technology, Xi'an 710048, People's Republic of China

[2] Key Laboratory of Materials Processing Engineering, College of Materials Science and Engineering, Xi'an Shiyou University, Xi'an 710065, People's Republic of China

[3] School of Materials Science and Engineering, Xi'an University of Sciences and Technology, Xi'an 710054, People's Republic of China

Published online: 05 August 2019

mode and doping concentrations of Cu^{2+}. For examples, if CuO is added in a form of KNN + x mol% CuO, double ferroelectric hysteresis loops can be obtained and retained until x = 0.2 [11]. However, if CuO is added in a form of $K_{0.5}Na_{0.5}(Nb_{1-2x/5}Cu_x)O_3$, with some Cu^{2+} entering into the interstitial sites, double ferroelectric hysteresis loops are exhibited in Cu-doped KNN ceramics with the Cu^{2+} concentration less than 1 mol%, while the 1.5 and 2 mol% Cu^{2+}-doped KNN ceramics show normal single loops [12]. It is generally accepted that this kind of double ferroelectric hysteresis loops characteristic is related to oxygen vacancy associated defect dipoles [7, 11, 12]. However, oxygen vacancies are not well designed in these two compositions mentioned above, and the corresponding mechanism should be further discussed.

Based on above analysis, the following formulation was designed: $K_{0.5}Na_{0.5}(Nb_{1-x}Cu_x)O_{3-3x/2}$, in which Cu^{2+} substituted Nb^{5+} at B-site and oxygen vacancies are created to make a charge balance. Then, oxygen vacancies can be controlled by adjusting the doping concentrations of Cu^{2+}. The effects of Cu^{2+} doping on ferroelectric properties are studied and the mechanism of oxygen vacancies on ferroelectric hysteresis loops is clarified.

2 Experimental procedure

Ceramic samples with the composition of $K_{0.5}Na_{0.5}(Nb_{1-x}Cu_x)O_{3-3x/2}$ (x = 0.005, 0.0075, 0.01, 0.0125, 0.015, 0.02 are abbreviated as KNNC5, KNNC7.5, KNNC10, KNNC12.5, KNNC15, KNNC20, respectively) are prepared by a solid state reaction method. The raw materials and purity used for sample preparation were: K_2CO_3(99%), Na_2CO_3(99.8%), Nb_2O_5(99.9%) and CuO (99.8%). The powders were weighted by a stoichiometric ratio and then mixed for 12 h with a rotation speed of 450 r/min by using a planetary ball milling machine with zirconia balls and ethanol as medium. Subsequently, the powders were dried and pressed into a cylinder in a diameter of 25 mm. Since the evaporation of K and Na has a large influence on the electrical properties of KNN [13, 14], the pressed cylinders are covered in a crucible and calcined at 850 °C and 900 °C for 2 h. After that, the calcinated powders were milled again for 12 h and dried. The dried powders were compacted into pellets in a thickness of 1 mm and a diameter of 10 mm and further pressed at 200 MPa for 5 min using a cold isostatic press machine. Finally, the pellets were embedded in self-source sacrificial powder and sintered at 1085–1095 °C for 4 h.

The density of the sintered pellets was measured by the Archimedes' immersion method. The phase and purity of the ceramics were studied by X-ray diffraction (XRD) (D/Max2550VBþ/PC, Rigaku, Tokyo, Japan). Rietveld refinements were carried out using the Fullprof program. The XRD data were collected in a 2θ range of 20–90° with a step size of 0.02° and a step time of 6 s to make a refinement. Orthorhombic $KNbO_3$ with Amm2 (ICSD-9533) atomic coordinates were used as the initial model. The microstructure such as grain size and homogeneity were investigated by using a field-emission scanning electron microscopy (FE-SEM) (JEOL-6700F, Japan Electron Co., Tokyo, Japan). Silver electrodes were painted on both sides of the polished surfaces and heated at 600 °C for 30 min. Temperature dependent permittivity (ε') and loss tangent (tanδ) were measured by a precision LCR meter (E4980, Agilent, Santa Clara, USA) associated with temperature controller (TP94, Linkam, Surrey, UK) from 500 to 25 °C with a cooling rate of 3 °C/min. Ferroelectric hysteresis loops were measured by using a ferroelectric test unit analyzer (TF-2000, AixACCT, Aachen, Germany) under 60 kV/cm at 1 Hz and room temperature.

3 Results and discussion

Figure 1 shows the curve between the relative density and sintering temperature. For KNNC5, KNNC7.5 and KNNC10, the relative density increases with the sintering temperature increasing. While for KNNC12.5, KNNC15 and KNNC20, the relative density first increases and then drops as the sintering temperature is above 1085 °C. Since copper has lower melting point, doping large concentration of Cu^{2+} might lead to the formation of liquid phase during the sintering, thus decreasing the relative density. These results indicate that the optimum sintering temperature of KNNC ceramics is 1095 °C (x ≤ 0.01) and 1085 °C (x ≥ 0.0125), respectively.

Figure 2 shows XRD patterns of KNNC ceramics. All the samples are typical orthogonal phase structure. There is no obvious impure phase detected when the doping

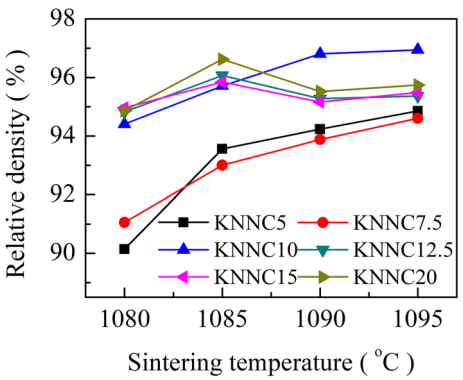

Fig. 1 The relative density as a function of sintering temperatures of KNNC ceramics

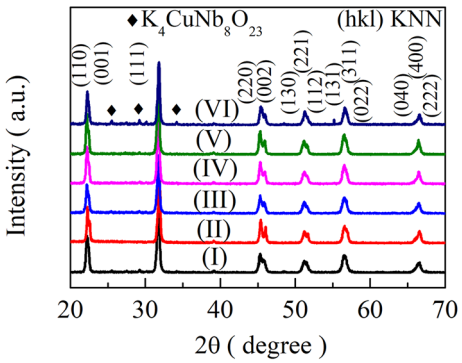

Fig. 2 XRD patterns of: (*I*) KNNC5, (*II*) KNNC7.5, (*III*) KNNC10, (*IV*) KNNC12.5, (*V*) KNNC15 and (*VI*) KNNC20

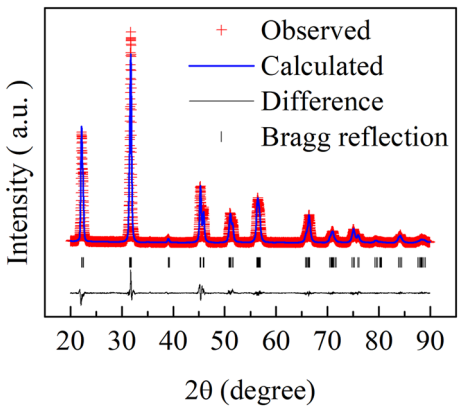

Fig. 3 XRD refinement result of KNNC12.5 (Color figure online)

concentration $x \leq 0.015$. However, the impurity phase $K_4CuNb_8O_{23}$ appears when the doping concentration $x = 0.02$, and the impurity phase accounts for 1.12 wt% in the total samples. As the doping amount of CuO increasing, the position of each characteristic peak in the XRD diffraction pattern does not change significantly, indicating that the lattice parameter of the sample does not change significantly due to the doping of CuO. This might be due to that the doping amount of Cu^{2+} is small, thus it is difficult for instrument to distinguish the tiny change of lattice parameters.

In order to confirm the occupied position of Cu^{2+}, XRD refinement was carried out on the specific sample of KNNC12.5. Figure 3 shows the experimental (cross-shaped), the fitted (blue line) and Bragg reflection values (blank bar), as well as the deviation between the calculated and observed intensity (blank line) of the KNNC12.5 ceramic. Well-fitting profiles are achieved, and the fitting factors, R_{wp}, R_p, and chi squared values (χ^2) are 10.8%, 7.84% and 2.53, indicating that Cu^{2+} locates at B-site as the formula of $K_{0.5}Na_{0.5}(Nb_{0.9875}Cu_{0.0125})O_{2.98125}$.

Figure 4 shows SEM images of KNNC ceramics with different Cu^{2+} doping concentrations. The grain size is 2.11 μm, 3.95 μm, 3.24 μm, 3.33 μm and 2.62 μm, for KNNC5, KNNC7.5, KNNC10, KNNC12.5 and KNNC15. The increased grain size can be attributed to the increased oxygen vacancy concentrations as the doping amount of Cu^{2+} increases, because oxygen vacancies can modify grain boundary mobility [15]. The grain size of KNNC150 abnormally decreases, which might be ascribed to the reason that there is trace account of impurities aggregated at the grain boundaries, inhibiting the grain boundary mobility [16], although the impure phase is not detected by XRD. This might be due to that the lower content of impurities is below the instrumental resolution.

Figure 5 shows temperature dependent permittivity for KNNC ceramics at 1 kHz, 10 kHz, 100 kHz and 1000 kHz. Tc and T_{O-T} show little variance with the Cu^{2+} concentrations increasing, which is in agreement with Ref. [17]. At low temperature, permittivity and dielectric loss are not dependent on frequencies, but at high temperature and low frequencies, all the samples show high permittivity and dielectric loss, which might be contributed from enhanced conductivity at high temperature. As the concentration of Cu^{2+} increases from 0.005 to 0.01, permittivity decreases from 325.1 to 291.9 and the dielectric loss decreases from 0.0195 to 0.0029 at room temperature and 1 kHz, suggesting that doping of Cu^{2+} in KNN at B-site results in a hardening effect. Nevertheless, permittivity and dielectric loos of KNNC12.5 and KNNC15 increase, which might be due to the increased conductivity or the grain size effect. It has been reported that the domain size is proportional to the grain size [18], thus KNNC15 has more domain boundaries, leading to high permittivity and dielectric loss. Dielectric properties and phase transition temperatures of KNNC ceramics are listed in Table 1.

Figure 6 exhibits P–E loops of KNNC ceramics under an electric field of 40 kV/cm. As can be seen from Fig. 4, all the samples show characteristic of double hysteresis loops, which is different from Ref. [12]. With the concentration of Cu^{2+} increasing, Ec increases from 3.98 to 11.1 kV/cm, which further confirms that the resulting hardening effect is due to the doping of Cu^{2+}. Figure 7 shows P–E loops of KNNC7.5 and KNNC15 ceramic under different electric fields. With the applied electric field increasing, the characteristic of double hysteresis loop for KNNC7.5 ceramic gradually disappears, but KNNC15 ceramic retains the characteristic of double hysteresis loop until 60 kV/cm. Liang [19] reported that the double hysteresis loop disappeared in the poled Cu^{2+} doped KNN ceramics, which also indicates that the double hysteresis is dependent on the applied electric field. The reason can be discussed in the following paragraph.

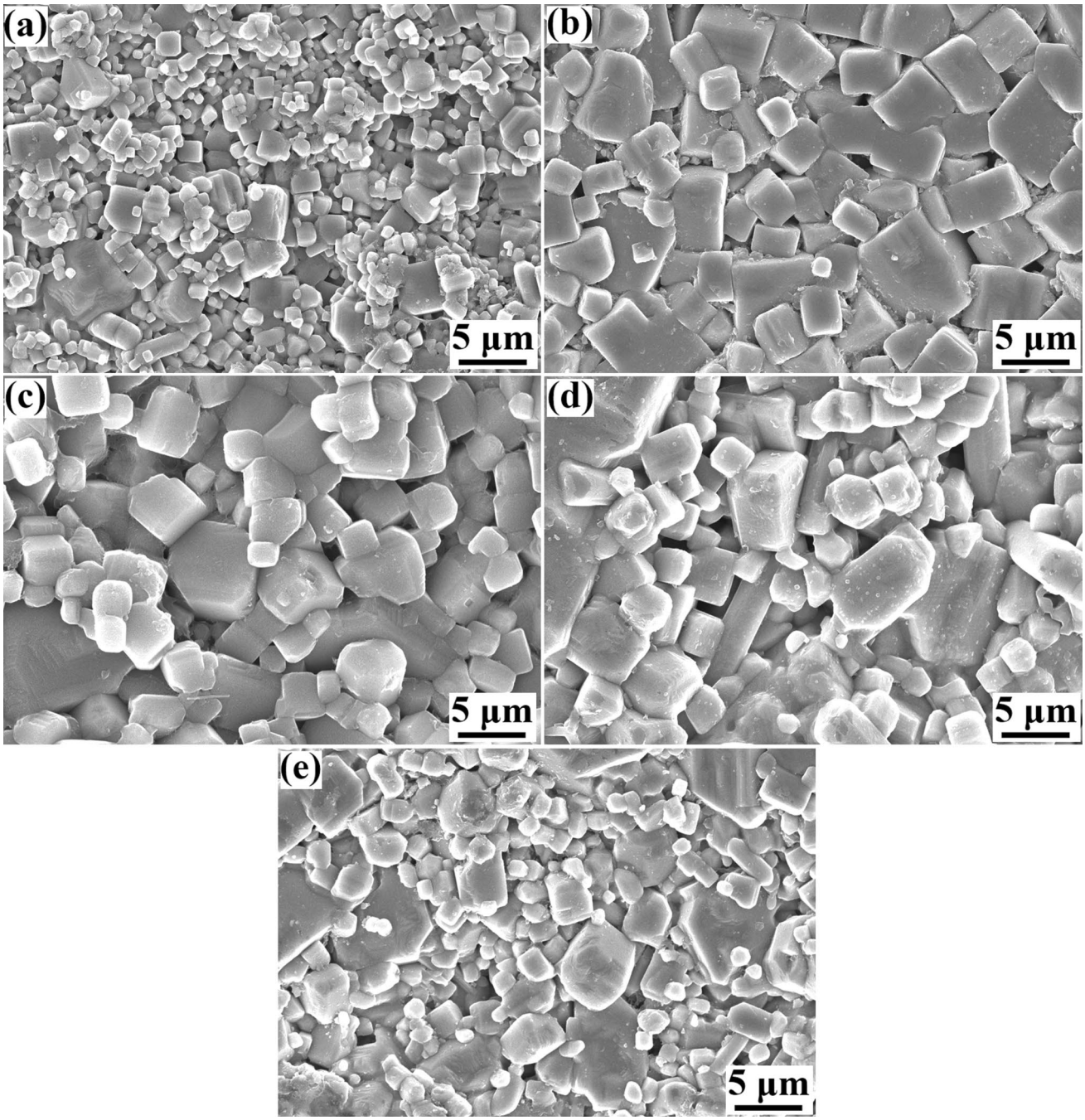

Fig. 4 SEM images of: **a** KNNC5, **b** KNNC7.5, **c** KNNC10, **d** KNNC12.5 and **e** KNNC15

Figure 8 shows the proposed mechanism of the ferroelectric behavior in KNNC ceramics. For pure KNN, as seen in Fig. 8a, it exhibits orthorhombic phase at room temperature, and the spontaneous polarization is along [011] direction. When B-site of KNN is substituted by a certain amount of Cu^{2+}, as shown in Fig. 8b, Cu^{2+} occupies Nb^{5+} position, and this kind of nonequivalent substitution produces a charged defect (Cu''''_{Nb}) and generates oxygen vacancies ($V_o^{\cdot\cdot}$). According to the symmetry conforming principle of point defects [20], the statistical distribution of $V_o^{\cdot\cdot}$ around Cu''''_{Nb} is not symmetric and affected greatly by the lattice symmetry. Because the phase transition from tetragonal to orthogonal phase is diffused in KNN [11], in an equilibrium state at room temperature, the symmetry of Cu''''_{Nb} and $V_o^{\cdot\cdot}$

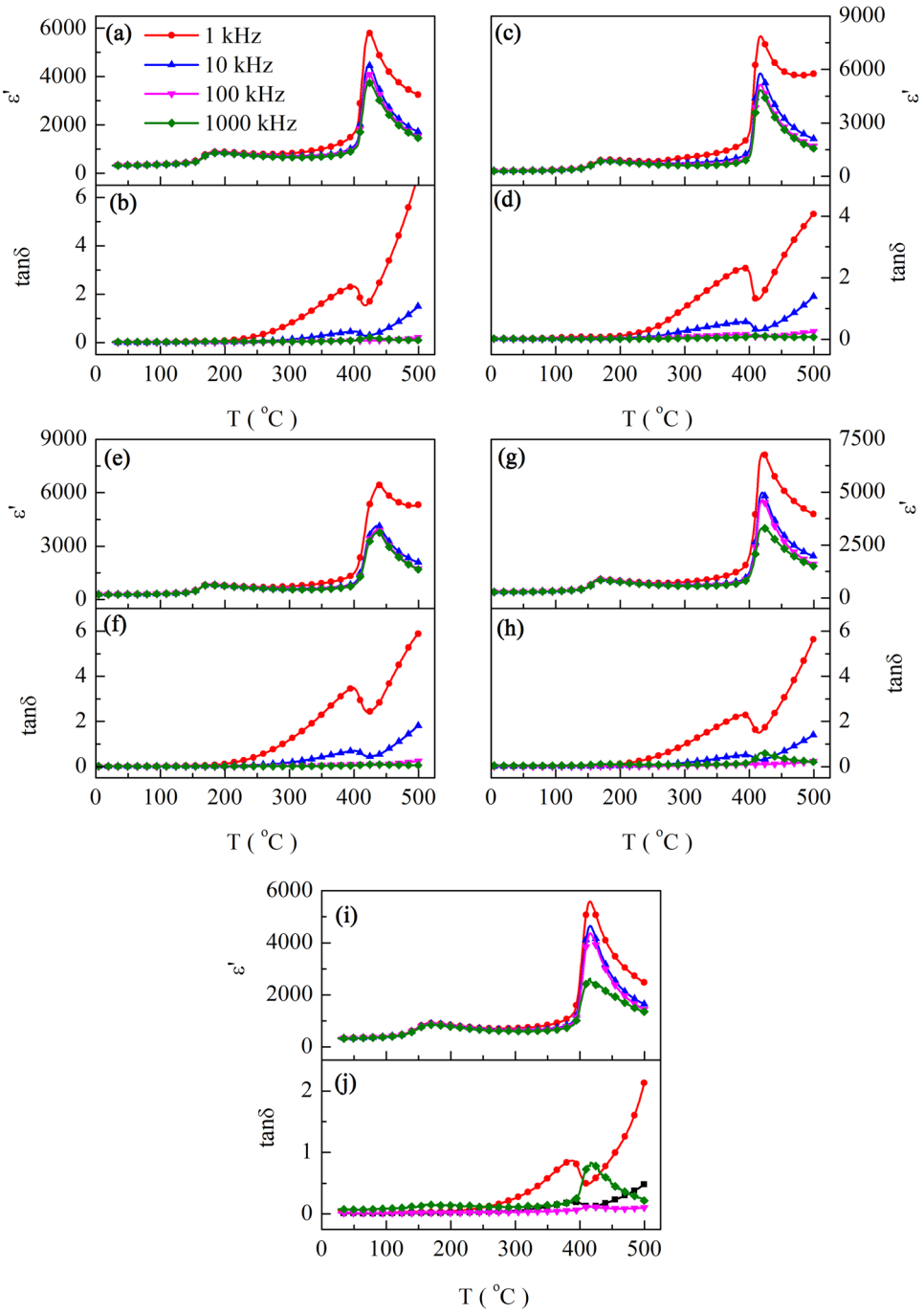

Fig. 5 Temperature dependent permittivity and dielectric loss of KNNC ceramics at different frequencies: **a**, **b** KNNC5, **c**, **d** KNNC7.5, **e**, **f** KNNC10, **g**, **h** KNNC12.5 and **i**, **j** KNNC15

Table 1 Dielectric properties and phase transition temperatures of KNNC ceramics

Samples	ε'	Tanδ	T_{O-T} (°C)	Tc (°C)
KNNC5	325.1	0.0195	167.3	423.3
KNNC7.5	312.4	0.0128	156.5	417.6
KNNC10	291.9	0.0029	162.3	429.4
KNNC12.5	289.0	0.0040	157.5	421.5
KNNC15	327.1	0.1378	156.5	418.5

also follows orthogonal symmetry. As a result, the defect dipole formed by the charged defect Cu_{Nb}''' and $V_o^{\cdot\cdot}$ is along the direction of spontaneous polarization. Under the applied electric field, as seen in Fig. 8c, the defect dipoles remain the [011] direction, but the spontaneous polarization is switched to the direction of applied electric field. Therefore, the defect dipole produces a restoring force to the switched polarization upon removal of the external field. Thus, the polarization disappears when the electric field is removed.

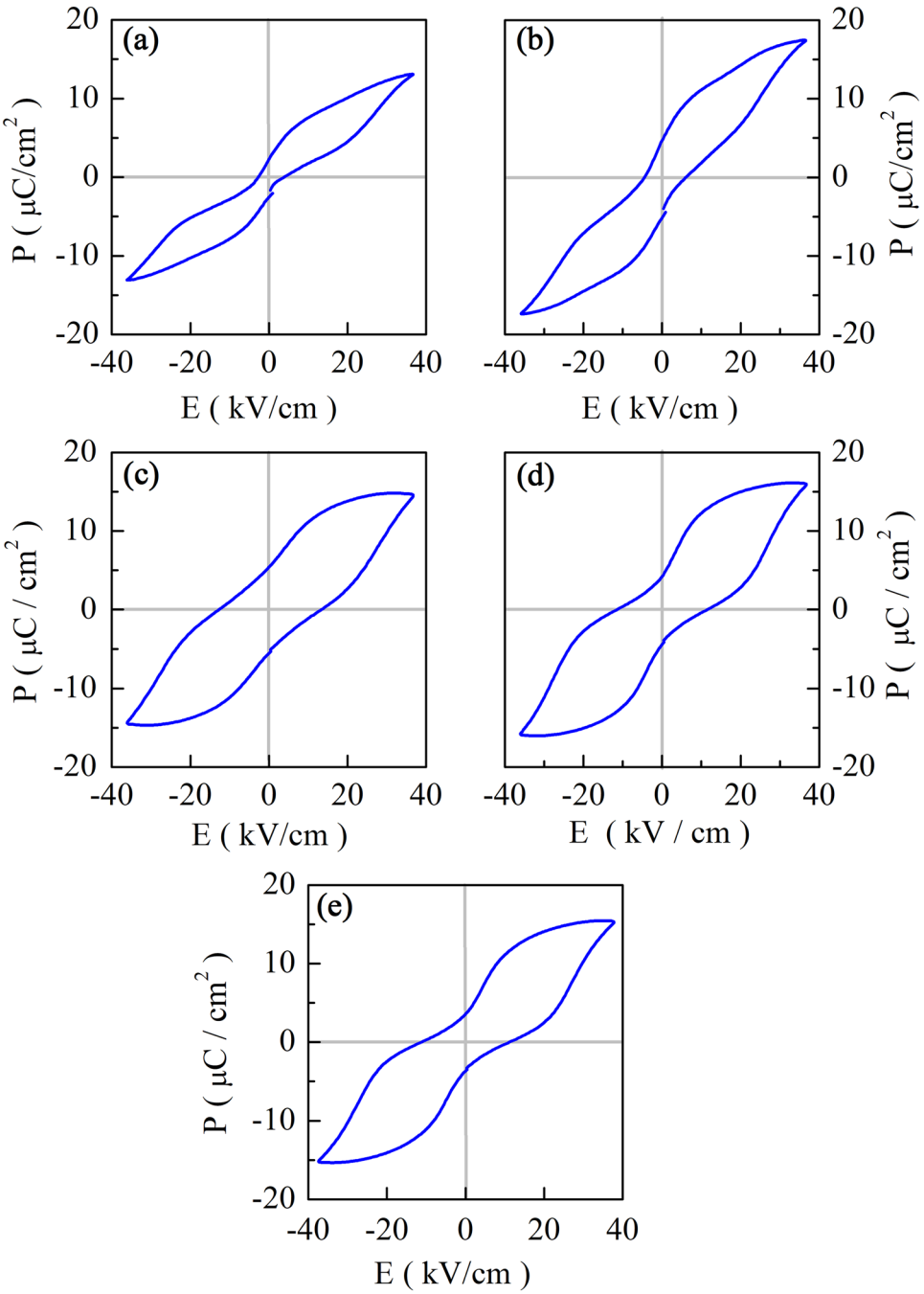

Fig. 6 P–E loops of Cu^{2+} B-site doped KNN ceramics under the electric field of 40 kV/cm: **a** KNNC5, **b** KNNC7.5, **c** KNNC10, **d** KNNC12.5 and **e** KNNC15

Macroscopically, the hysteresis loop exhibits a characteristic of double hysteresis loop. Although double hysteresis loops were also observed in $K_{0.5}Na_{0.5}(Nb_{1-2x/5}Cu_x)O_3$ [12]. In this case x some Cu^{2+} substituted Nb^{5+} and the others are located at interstitial sites, thus oxygen vacancies are created mainly by the evaporation of K^+ and Na^+. Consequently, the defect dipoles are limited and the charges of defect dipole ($Cu''''_{Nb} - V^{\cdot\cdot}_o$) might be balanced by interstitial $Cu^{\cdot\cdot}_i$. As a result, double hysteresis loops disappear at the large concentration of Cu^{2+}.

Besides, in our case, at lower Cu^{2+} doping concentrations when a sufficiently large applied electric field is applied, the applied electric field could be sufficient to overcome the restoring force generated by the defective dipole, the P–E loop restores to the normal hysteresis loop. However, at higher Cu^{2+} doping concentrations,

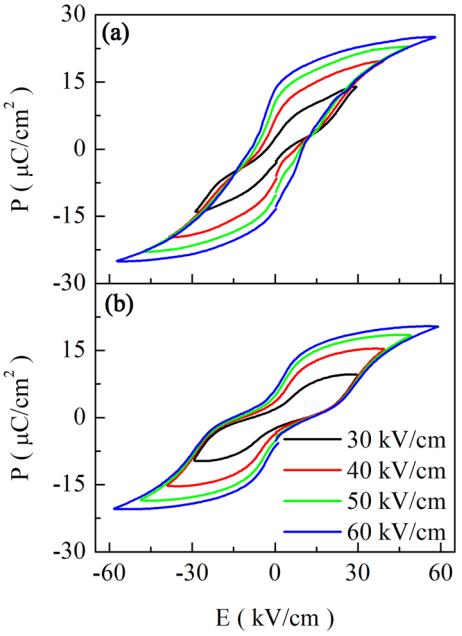

Fig. 7 P–E loops of Cu^{2+} B-site doped KNN ceramics under different applied electric fields: **a** KNNC7.5 and **b** KNNC15

the applied electric field is not sufficient to overcome the restoring force generated by the defective dipole, therefore, the P–E loop retains the double hysteresis loop.

4 Conclusions

$K_{0.5}Na_{0.5}(Nb_{1-x}Cu_x)O_{3-1.5x}$ ceramics were prepared by a solid state method. The dielectric, ferroelectric behavior and defect compensation mechanism were studied. The doping of Cu^{2+} in KNN leads to a hardening effect, that is permittivity and dielectric loss decreases, and the coercive field increases with the concentration of Cu^{2+} increasing. All ceramics exhibit double hysteresis loop characteristics when the doping concentration of $x = 0.05 \sim 0.15$. But this kind of double hysteresis loop is dependent on the applied electric field. The characteristic of double hysteresis loop for KNNC7.5 ceramic disappears above 50 kV/cm, but KNNC15 ceramic retains the characteristic of double hysteresis loop until 60 kV/cm. The corresponding mechanism is proposed. In Cu^{2+} doped KNN, $(Cu''''_{Nb} - V^{\cdot\cdot}_{o})$ defect complex is created and provides a driving force for domain back switching, which is origin for the characteristic of double hysteresis loop. But at lower Cu^{2+} doping concentrations, the higher applied electric field could be sufficient to overcome the restoring force generated by the defective dipole, therefore P–E loop restores to the normal hysteresis loop.

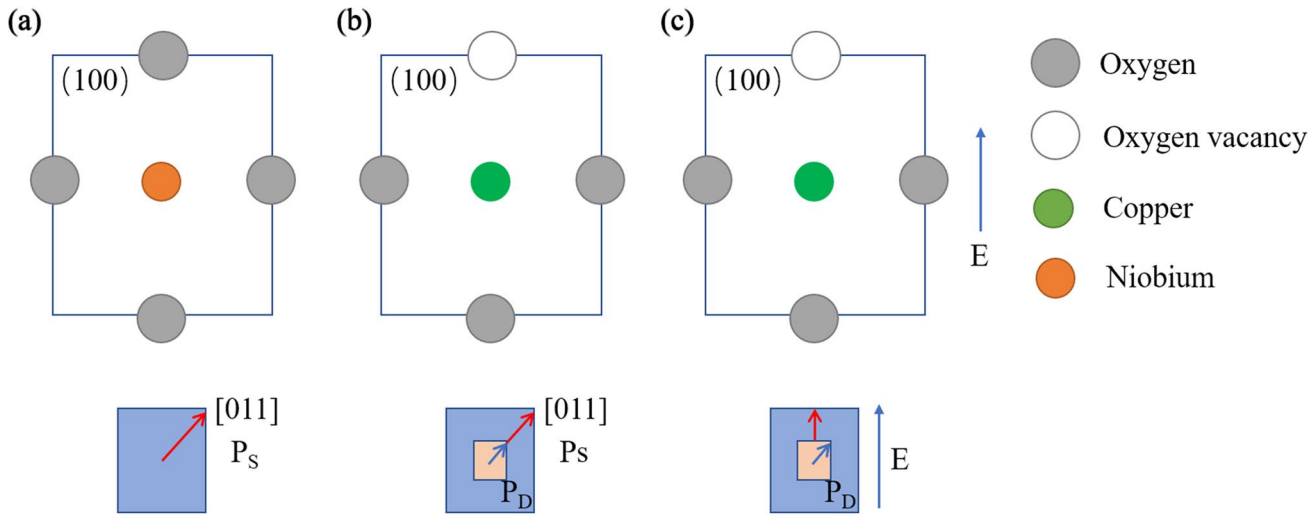

Fig. 8 The proposed mechanism defect dipole on P–E loops of Cu^{2+} substituted KNN ceramics: **a** pure KNN, **b**, **c** Cu^{2+} B-site substituted KNN ceramics

Acknowledgements This work was financially supported by National Natural Science Foundation of China (51802246), Natural Science Basic Research Plan in Shaanxi Province of China (2018JQ5110), State Key Laboratory of Solidification Processing in NWPU (SKLSP201839), Fund Program of the Scientific Activities of Selected Returned Overseas Professionals in Shaanxi Province, Special Scientific Research Plan Projects of Shaanxi Education Department (17JK0382) and Scientific and Technological Project of Yulin City (2016-16-6).

References

1. K. Uchino, *Ferroelectric Devices* (Marcel Dekker Inc, New York, 2000), pp. 1–10
2. B. Jaff, *Piezoelectric Ceramics* (Academic Press, London, 1971), pp. 151–161
3. J.E. Garcia, R. Pérez, A. Albareda, J.A. Eiras, Non-linear dielectric and piezoelectric response in undoped and Nb^{5+} or Fe^{3+} doped PZT ceramic system. J. Eur. Ceram. Soc. **27**, 4029–4032 (2007)
4. J. Rödel, K.G. Webber, R. Dittmer, W. Jo, M. Kimurac, D. Damjanovic, Transferring lead-free piezoelectric ceramics into application. J. Eur. Ceram. Soc. **35**, 1659–1681 (2015)
5. T.R. Shrout, S.J. Zhang, Lead-free piezoelectric ceramics: alternatives for PZT? J. Electroceram. **19**, 111–124 (2007)
6. L.J. Liu, D.P. Shi, L.L. Fan, J. Chen, G.Z. Li, L. Fang, B. Elouadi, Ferroic properties of Fe-doped and Cu-doped $K_{0.45}Na_{0.49}Li_{0.06}NbO_3$ ceramics. J. Mater. Sci. **26**, 6592–6598 (2015)
7. N.M. Hagh, K. Kerman, B. Jadidian, A. Safari, Dielectric and piezoelectric properties of Cu^{2+}-doped alkali niobates. J. Eur. Ceram. Soc. **29**, 2325–2332 (2009)
8. D. Lin, K.W. Kwok, H.L.W. Chan, Piezoelectric and ferroelectric properties of Cu-doped $K_{0.5}Na_{0.5}NbO_3$ lead-free ceramics. J. Phys. D **41**, 045401 (2008)
9. S. Körbel, P. Marton, C. Elsässer, Formation of vacancies and copper substitutionals in potassium sodium niobate under various processing conditions. Phys. Rev. B **81**, 174115 (2010)
10. A. Shigemi, T. Wada, Evaluations of phases and vacancy formation energies in $KNbO_3$ by first-principles calculation. Jpn. J. Appl. Phys. **44**(Part 1), 8048–8054 (2005)
11. D. Lin, K.W. Kwok, H.L.W. Chan, Double hysteresis loop in Cu-doped $K_{0.5}Na_{0.5}NbO_3$ lead-free piezoelectric ceramics. Appl. Phys. Lett. **90**, 232903 (2007)
12. S.M. Ke, H.T. Huang, H.Q. Fan, H.K. Lee, L.M. Zhou, Y.W. Mai, Antiferroelectric-like properties and enhanced polarization of Cu-doped $K_{0.5}Na_{0.5}NbO_3$ piezoelectric ceramics. Appl. Phys. Lett. **101**, 082901 (2012)
13. L.J. Liu, H.Q. Fan, L. Fang, X.L. Chen, H. Dammak, M.P. Thi, Effects of Na/K evaporation on electrical properties and intrinsic defects in $Na_{0.5}K_{0.5}NbO_3$ ceramics. Mater. Chem. Phys. **117**, 138–141 (2009)
14. X. Liu, Y.X. Zhao, J. Shi, H.L. Du, X.M. Xu, H. Lu, J.F. Che, X.Y. Li, Improvement of dielectric and ferroelectric properties in bismuth sodium titanate based relaxors through Bi non-stoichiometry. J. Alloys Compd. **799**, 231–238 (2019)
15. Y. Jung, S.Y. Choi, S.J.L. Kang, Effect of oxygen partial pressure on grain boundary structure and grain growth behavior in $BaTiO_3$. Acta Mater. **54**, 2849–2855 (2006)
16. P.R. Ren, Z.C. Liu, X. Wang, Z.F. Duan, Y.H. Wan, F.X. Yan, G.Y. Zhao, Dielectric and energy storage properties of $SrTiO_3$ and $SrZrO_3$ modified $Bi_{0.5}Na_{0.5}TiO_3$–$Sr_{0.8}Bi_{0.1}\square_{0.1}TiO_3$ based ceramics. J. Alloys Compd. **742**, 683–689 (2018)
17. X.H. Tan, H.Q. Fan, S.M. Ke, L.M. Zhou, Y.W. Mai, H.T. Huang, Structural dependence of piezoelectric, dielectric and ferroelectric properties of $K_{0.5}Na_{0.5}(Nb_{1-2x/5}Cu_x)O_3$ lead-free ceramics with high Qm. Mater. Res. Bull. **47**, 4472–4477 (2012)
18. G. Arlt, D. Hennings, G. Dewith, Dielectric properties of fine-grained barium-titanate ceramics. J. Appl. Phys. **58**, 1619–1625 (1985)
19. W.F. Liang, D.Q. Xiao, J.G. Wu, W.J. Wu, J.G. Zhu, Origin of high mechanical quality factor in CuO-doped (K, Na)NbO_3-based ceramics. Front. Mater. Sci. **8**, 165–175 (2014)
20. X. Ren, Large electric-field-induced strain in ferroelectric crystals by point-defect-mediated reversible domain switching. Nat. Mater. **3**, 91–94 (2004)